Science Advances
AAAS

# Supplementary Materials for

## Superconductivity in an ultrathin multilayer nickelate

Xi Yan *et al.*

Corresponding author: Hua Zhou, hzhou@anl.gov; Dillon D. Fong, fong@anl.gov

*Sci. Adv.* **11**, eado4572 (2025)
DOI: 10.1126/sciadv.ado4572

**This PDF file includes:**

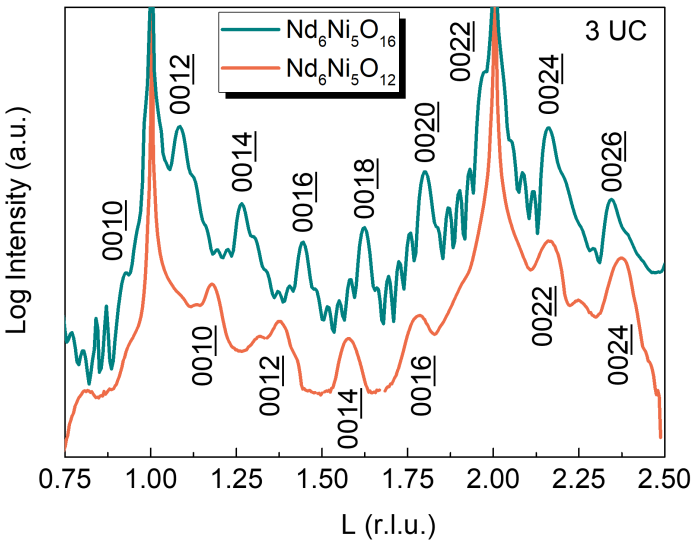


Figure S1: The specular Bragg rods of $Nd_6Ni_5O_{16}$ and $Nd_6Ni_5O_{12}$. The 3 UC $Nd_6Ni_5O_{16}$ film is grown by employing the NdO $\rightarrow$ NdO $\rightarrow$ NdO $\rightarrow$ $NiO_2$ stacking sequence. The superlattice peaks of the $Nd_6Ni_5O_{16}$ film shift rightward after the topotactic reduction, forming a superconducting $Nd_6Ni_5O_{12}$ reduced phase.

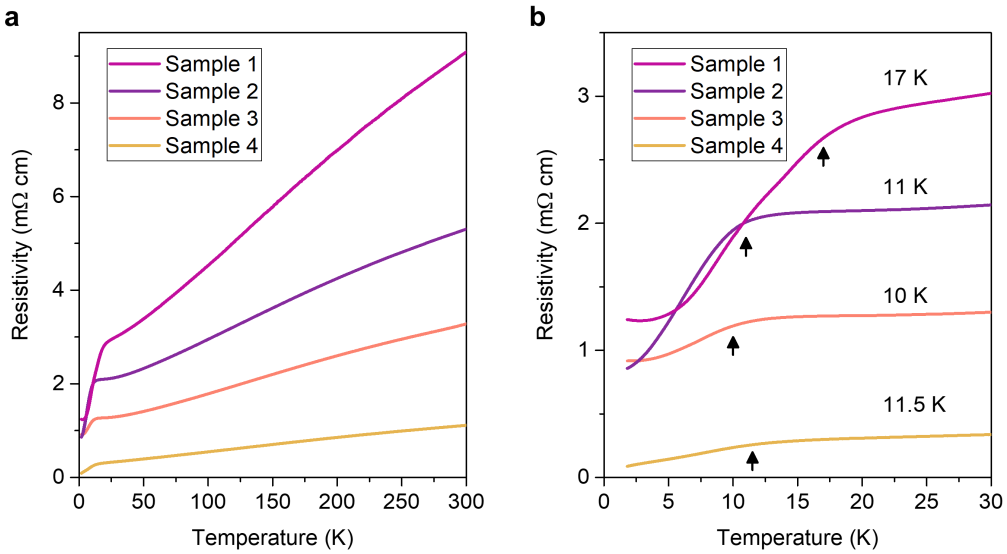


Figure S2: The temperature-dependent resistivity for multiple $Nd_6Ni_5O_{12}$ samples. All of them are 1 UC and are measured down to 1.8 K. (a) The superconducting correlations are observed on both the *in situ* reduced sample (Sample 1) as well as three different *ex situ* reduced samples (Samples 2-4). The onset of superconductivity ranges from 13 K to 22 K. (b) The enlarged region for (a) from 0 K to 30 K. The points of maximum curvature for the 4 samples are described in the figure. The resistivity of the superconducting thin films can be affected by various factors, including the quality of the parent phase and the reduction conditions, specifically, reduction temperature and reduction time. This can lead to sample-to-sample variations even with the same film thickness.

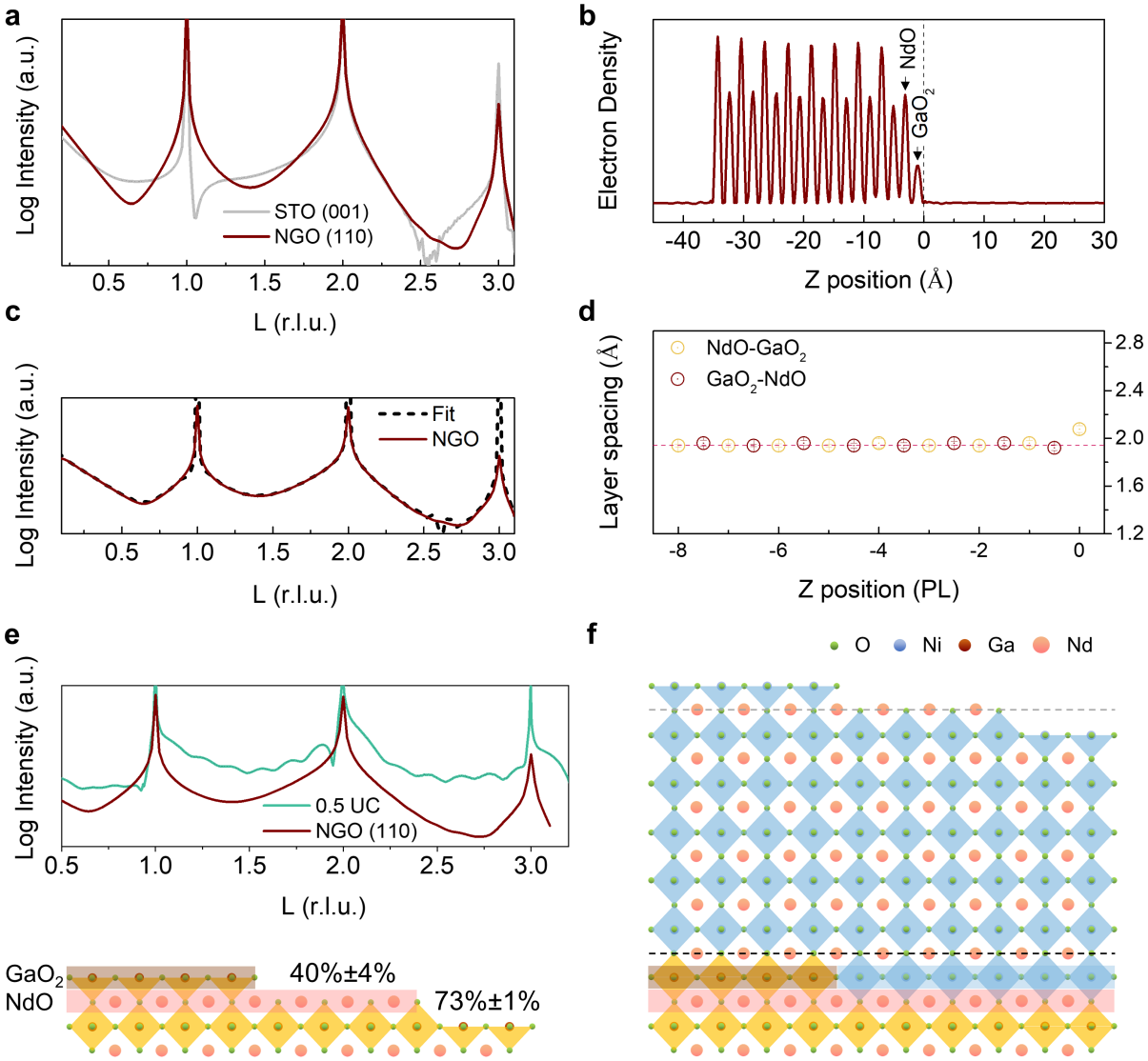


Figure S3: The CTRs of the substrates and COBRA results for NGO (110) substrate. (a) The structural factor contribution of $TiO_2$ double-layer on the surface of a $SrTiO_3$ (STO) (001) substrate can cause a sharp intensity minimum at $L = 1.05$ r.l.u. on its CTR. The absence of this sharp minimum on NGO (110) substrate indicates a mixed surface termination with NdO and $GaO_2$. (b) (c) The COBRA fitting and the electron density profiles along the out-of-plane direction, $z$ extracted from COBRA for the NGO (110) substrate. (d) The layer spacings between every NdO and $GaO_2$ planes extracted from the COBRA derived electron density profile. (e, f) The specular Bragg rod (measured at 560°C) and the resulting crystal structures as determined by COBRA, for the initial $NdGaO_3$ substrate (with the structure shown at the bottom of (e)) and after growth of the initial $\frac{1}{2}$ UC of the $Nd_6Ni_5O_{16}$ film (with the structure shown in (f)).

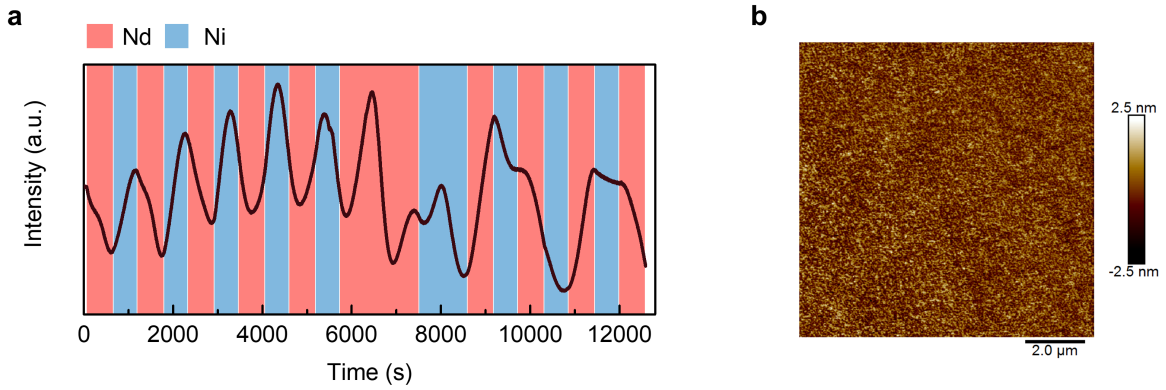


Figure S4: The $00\frac{1}{2}$ intensity measured by X-ray scattering during growth and an atomic force microscope (AFM) image of the final surface. (a) The $Nd_6Ni_5O_{16}$ films are grown by a shutter growth sequence starting with a NdO layer. The oscillations monitored at the surface sensitive $00\frac{1}{2}$ r.l.u. position for the the first five unit cells of $NdNiO_3$ and a NdO adlayer (0.5 UC of $Nd_6Ni_5O_{16}$ film) demonstrate a layer-by-layer growth mode. (b) The AFM image of the 1 UC $Nd_6Ni_5O_{16}$ film before reduction with a scan area of 10 $\mu$m $\times$ 10 $\mu$m. The root mean square (RMS) roughness is 0.616 nm.

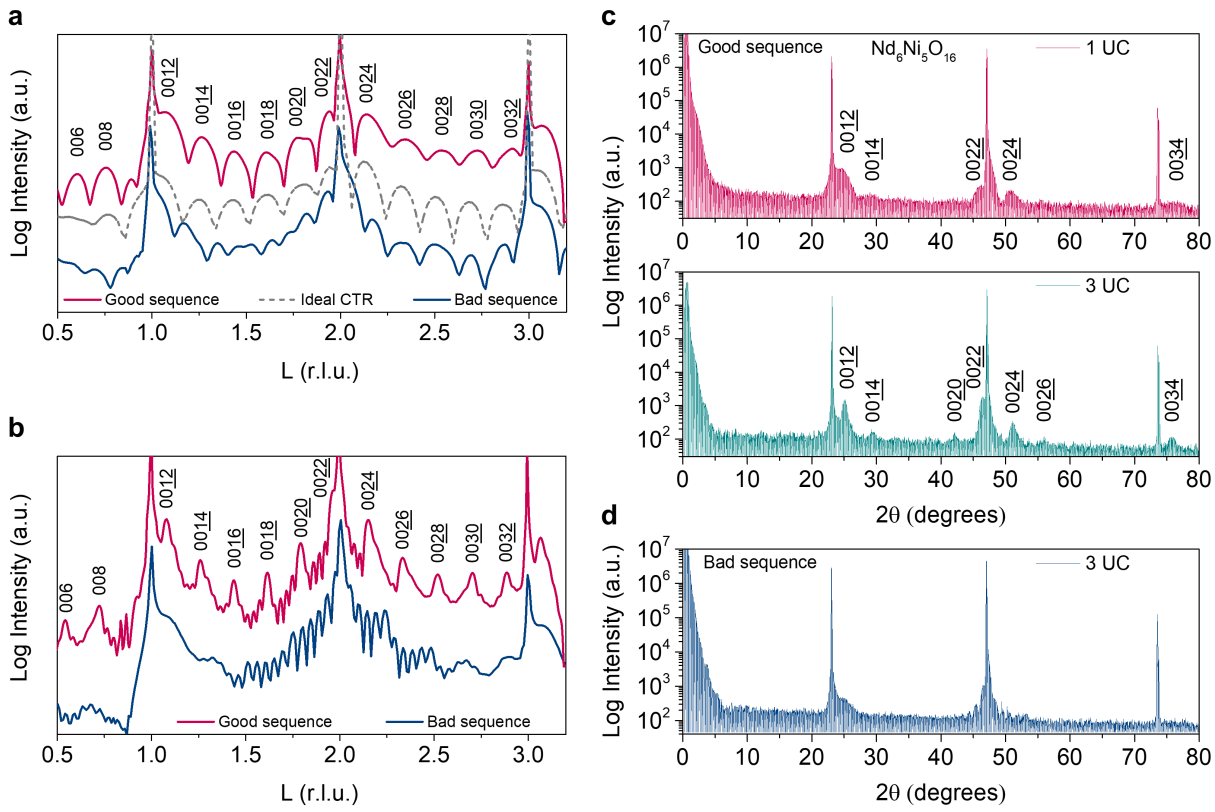


Figure S5: CTRs for different growth sequences. (a) CTRs for the 1 UC $Nd_6Ni_5O_{16}$ films deposited according to two different stacking sequences. The dashed, gray curve is the ideal CTR calculated assuming singly-terminated NGO, with NdO termination. After growing a 0.5 UC $Nd_6Ni_5O_{16}$ film, the subsequent growth of NdO $\rightarrow$ NdO $\rightarrow$ $NiO_2$ results in a dynamic layer rearrangement, forming a mis-stacking structure (blue curve, bad sequence); while adding an NdO adlayer on top of the rock salt slab, that is, NdO $\rightarrow$ NdO $\rightarrow$ NdO $\rightarrow$ $NiO_2$, leads to a specular Bragg rod (red curve, good sequence) very similar to the calculated 00$L$ for the 1 UC $Nd_6Ni_5O_{16}$ film. (b) The comparison of the 3 UC $Nd_6Ni_5O_{16}$ films grown by the two different deposition sequences further exhibits the necessity of the additional NdO layer. (c) Lab source XRD for 1 UC and 3 UC $Nd_6Ni_5O_{16}$ films grown in NdO $\rightarrow$ NdO $\rightarrow$ NdO $\rightarrow$ $NiO_2$ sequence. (d) Lab source XRD for the 3 UC nickelate film deposited in NdO $\rightarrow$ NdO $\rightarrow$ $NiO_2$ sequence.

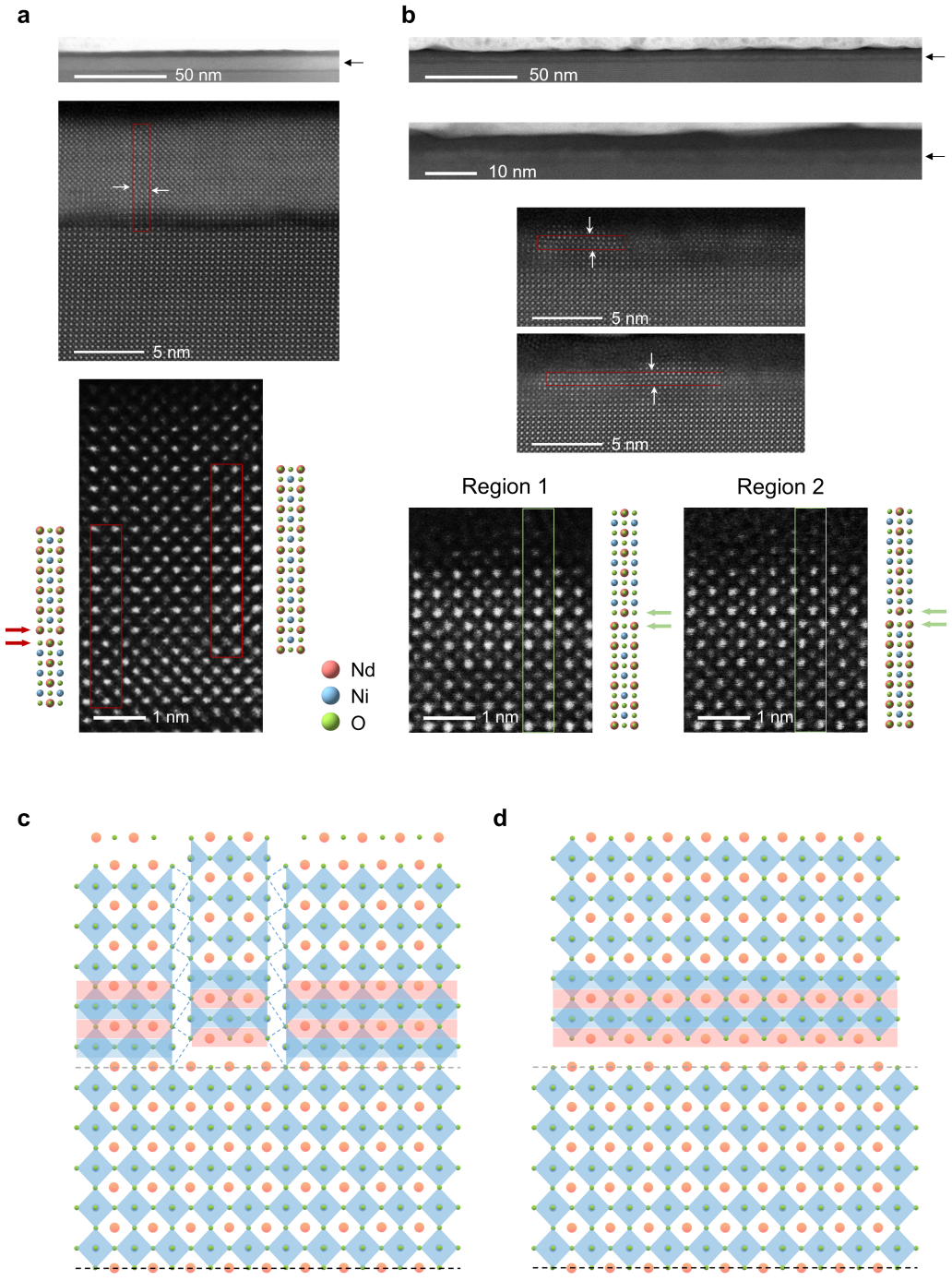


Figure S6: Structural characterization of the layered nickelates. (a, b) High-angle annular dark-field scanning transmission electron microscopy (STEM) images for films grown with the NdO $\rightarrow$ NdO $\rightarrow$ $NiO_2$ sequence (1 UC) and the NdO $\rightarrow$ NdO $\rightarrow$ NdO $\rightarrow$ $NiO_2$ sequence (3 UC). The black arrows point to the film. The rock salt layers are marked by red and green arrows. Stacking faults are indicated by the white arrows. (c, d) Schematics of the structures grown in NdO $\rightarrow$ NdO $\rightarrow$ $NiO_2$ and NdO $\rightarrow$ NdO $\rightarrow$ NdO $\rightarrow$ $NiO_2$ sequences, respectively.

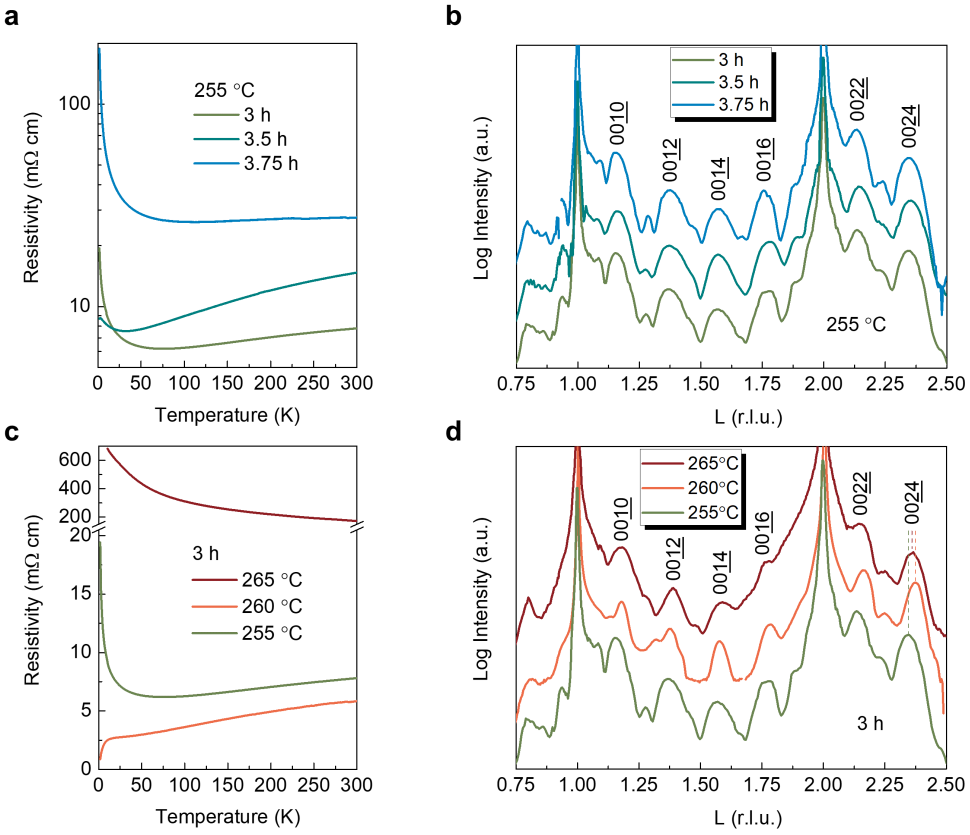


Figure S7: The *ex situ* reduction experiments on the 3 UC samples. (a)(b) The effect of the reduction time on the resistivity properties and the corresponding CTRs. At a fixed reduction temperature of 255°C, the metal-insulator transition temperatures for the films reduced for 3 hours, 3.5 hours and 3.75 hours are 76 K, 32 K and 112 K, respectively. (c) The effect of the reduction temperature on the resistivity properties. By varying the reduction temperature from 255°C to 265°C in increments of 5°C when fixing a reduction time of 3 hours, the films transform from a semiconducting state to a superconducting state (260°C), ending with an insulating state. (d) The CTRs measured after being reduced in different reduction temperatures. The specular Bragg rod of the superconducting sample shows the sharpest Bragg peaks and the smallest out-of-plane lattice constant among all the samples (see the 00$\underline{24}$ peak shown at the right).

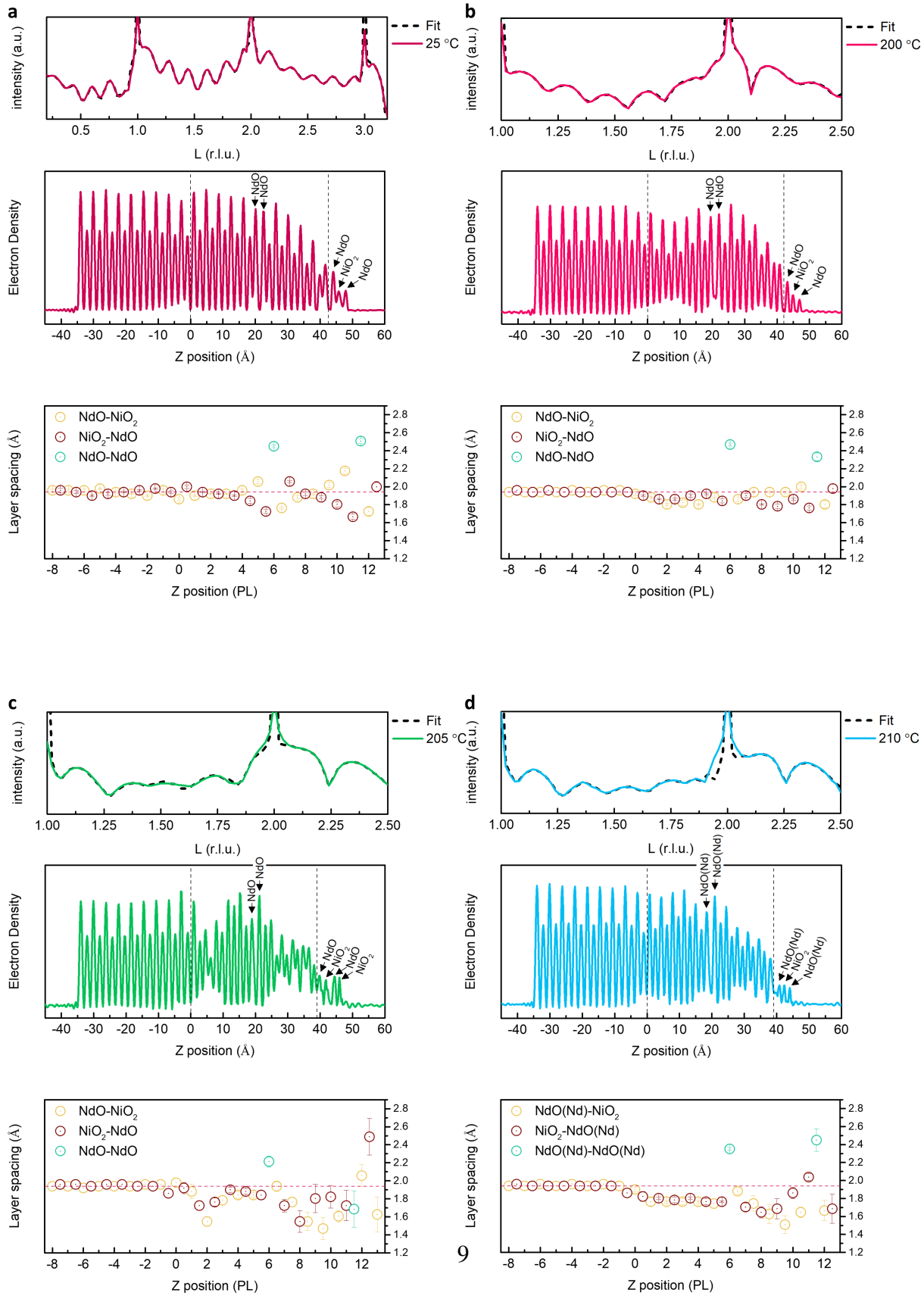
a
b
c
d
intensity (a.u.)
L (r.l.u.)
Fit
25 °C
200 °C
205 °C
210 °C
Electron Density
Z position (Å)
NdO
NiO2
NdO(Nd)
Layer spacing (Å)
Z position (PL)
NdO-NiO2
NiO2-NdO
NdO-NdO
NdO(Nd)-NiO2
NiO2-NdO(Nd)
NdO(Nd)-NdO(Nd)

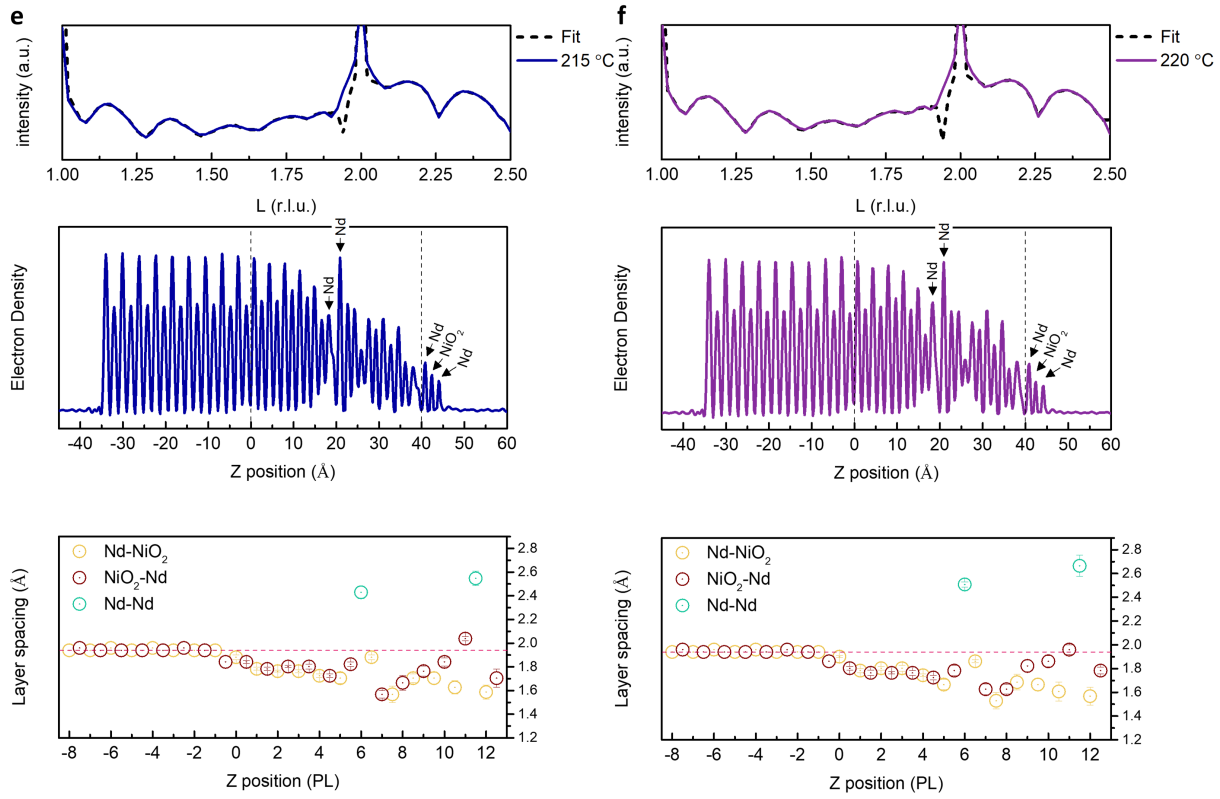


Figure S8: Detailed COBRA analysis for the 1 UC nickelate sample. The *in situ* CTRs, the electron density profiles along the out-of-plane direction, $z$, and the layer spacings taken at the reduction temperatures of (a) room temperature, t = 0 min (b) 200°C, t = 97 min (c) 205°C, t = 220 min (d) 210°C, t = 269 min (e) 215°C, t = 308 min and (f) 220°C, t = 328 min, respectively. Here, the layer spacing refers to the distance between each respective atomic layer, AO-$BO_2$, $BO_2$-AO and AO-AO. The time intervals are calculated from the start time for each scan.

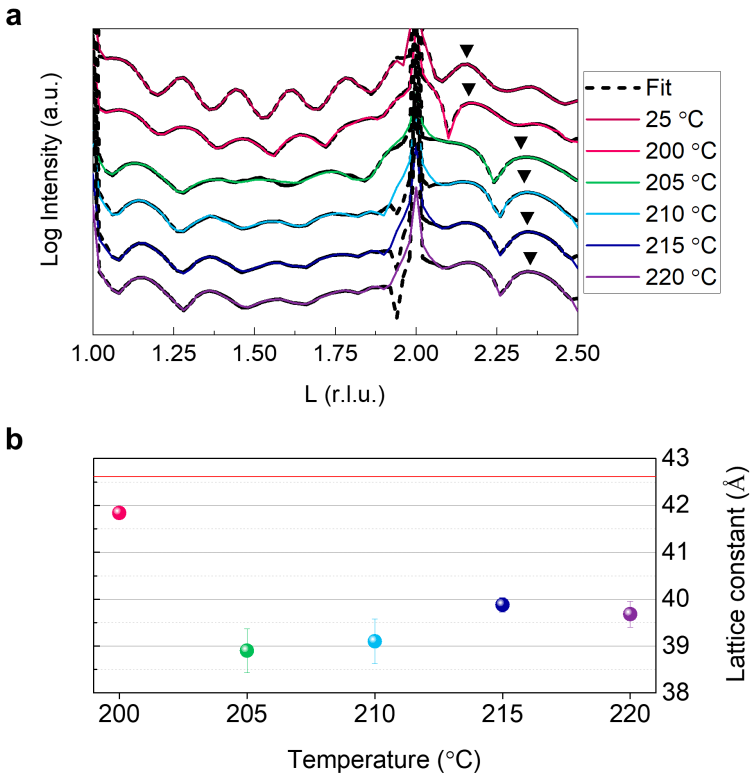


Figure S9: The summary of the *in situ* CTRs and their COBRA fitting curves at different reduction temperatures (a) and the lattice constants of the full unit cell during reduction (b) for the 1 UC nickelate film. The triangles in (a) track the evolution of the 00$\underline{24}$ peak during reduction. The red line in (b) refers to the lattice constant at 25°C.

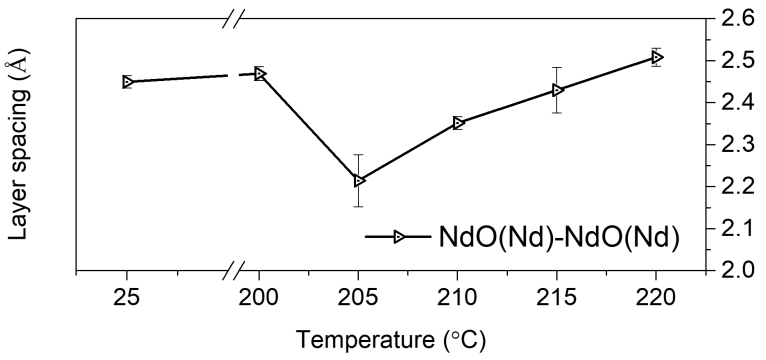


Figure S10: The layer spacing between the NdO (or Nd after reduction) layers in the middle of the 1 UC nickelate film at different reduction temperature. The reduction process converts the rock salt $Nd_2O_2$ layers to the fluorite structure.

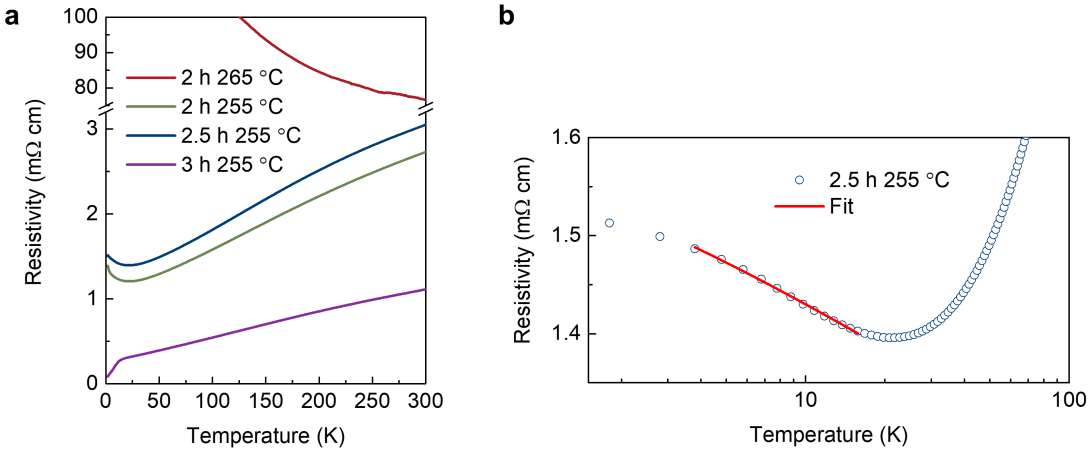


Figure S11: The *ex situ* reduction experiments on the 1 UC samples. (a) The $\rho$(T) profiles after different reduction conditions. 2 hours of reduction at a higher reduction temperature (265°C) results in an insulating state. The semiconducting states are achieved after 2 hours and 2.5 hours of reduction at 255°C, while further reducing the film for 3 hours leads to superconductivity. (b) When approaching the superconductivity, the logarithmic temperature dependence of the resistivity is observed. The resistivity is approximately linear in the temperature range of $\sim$ 4 K to $\sim$ 15 K, and saturation is observed below 4 K. Similar behaviors were observed in undoped $LaNiO_2$ films and the underdoped $R_{1-x}Sr_xNiO_2$ systems (4, 16, 17, 40, 41).

The logarithmic behaviors at low temperatures in Figure S11 may be theoretically conceived from Kondo spin singlets in $NdNiO_2$ formed by incorporating the Kondo coupling between the low-density Nd 5*d* conduction electrons and the localized Ni $3d_{x^2-y^2}$ electrons to the $t-J$ model for cuprates (51). Alternatively, given the possible presence of inhomogeneities in our samples, as indicated by the lack of a zero Ohm state, combined with the presence of disorder holes in the $NiO_2$ planes, localization effects cannot be precluded. We notice that in the Sr-doped infinite-layer nickelates, the logarithmic temperature dependence is relatively insensitive to disorder strength (52). Additional measurements like magnetoresistance or temperature dependence of the Hall coefficient could aid in differentiating between these two effects. A two-band model with both electron and hole carriers was proposed due to a relatively small magnetoresistance and negative Hall coefficients in the Sr-doped nickelate system (16). However, distinct from the

Sr-doped nickelates, Hall coefficients remain positive at all temperatures for the reduced multilayer nickelate, suggesting a single-band scenario. Therefore, in order to investigate intrinsic transport mechanisms, further efforts in minimizing disorder and reducing extrinsic defects are required.

## REFERENCES AND NOTES


1. M. R. Norman, Entering the nickel age of superconductivity. *Physics* **13**, 85 (2020).

2. W. E. Pickett, The dawn of the nickel age of superconductivity. *Nat. Rev. Phys.* **3**, 7–8 (2021).

3. D. Li, K. Lee, B. Y. Wang, M. Osada, S. Crossley, H. R. Lee, Y. Cui, Y. Hikita, H. Y. Hwang, Superconductivity in an infinite-layer nickelate. *Nature* **572**, 624–627 (2019).

4. M. Osada, B. Y. Wang, B. H. Goodge, S. P. Harvey, K. Lee, D. Li, L. F. Kourkoutis, H. Y. Hwang, Nickelate superconductivity without rare-earth magnetism: (La,Sr)$NiO_2$. *Adv. Mater.* **33**, e2104083 (2021).

5. B. Y. Wang, D. Li, B. H. Goodge, K. Lee, M. Osada, S. P. Harvey, L. F. Kourkoutis, M. R. Beasley, H. Y. Hwang, Isotropic Pauli-limited superconductivity in the infinite-layer nickelate $Nd_{0.775}Sr_{0.225}NiO_2$. *Nat. Phys.* **17**, 473–477 (2021).

6. Z. Chen, M. Osada, D. Li, E. M. Been, S.-D. Chen, M. Hashimoto, D. Lu, S.-K. Mo, K. Lee, B. Y. Wang, F. Rodolakis, J. L. McChesney, C. Jia, B. Moritz, T. P. Devereaux, H. Y. Hwang, Z.-X. Shen, Electronic structure of superconducting nickelates probed by resonant photoemission spectroscopy. *Matter* **5**, 1806–1815 (2022).

7. J. Fowlie, M. Hadjimichael, M. M. Martins, D. Li, M. Osada, B. Y. Wang, K. Lee, Y. Lee, Z. Salman, T. Prokscha, J.-M. Triscone, H. Y. Hwang, A. Suter, Intrinsic magnetism in superconducting infinite-layer nickelates. *Nat. Phys.* **18**, 1043–1047 (2022).

8. S. W. Zeng, X. M. Yin, C. J. Li, L. E. Chow, C. S. Tang, K. Han, Z. Huang, Y. Cao, D. Y. Wan, Z. T. Zhang, Z. S. Lim, C. Z. Diao, P. Yang, A. T. S. Wee, S. J. Pennycook, A. Ariando, Observation of perfect diamagnetism and interfacial effect on the electronic structures in infinite layer $Nd_{0.8}Sr_{0.2}NiO_2$ superconductors. *Nat. Commun.* **13**, 743 (2022).

9. X. Ding, C. C. Tam, X. Sui, Y. Zhao, M. Xu, J. Choi, H. Leng, J. Zhang, M. Wu, H. Xiao, X. Zu, M. Garcia-Fernandez, S. Agrestini, X. Wu, Q. Wang, P. Gao, S. Li, B. Huang, K.-J. Zhou, L. Qiao, Critical role of hydrogen for superconductivity in nickelates. *Nature* **615**, 50–55 (2023).

10. W. Wei, D. Vu, Z. Zhang, F. J. Walker, C. H. Ahn, Superconducting $Nd_{1-x}Eu_xNiO_2$ thin films using in situ synthesis. *Sci. Adv.* **9**, eadh3327 (2023).

11. T. Xie, Z. Liu, C. Cao, Z. Wang, J. Yang, W. Zhu, Microscopic theory of superconducting phase diagram in infinite-layer nickelates. *Phys. Rev. B* **106**, 035111 (2022).

12. C.-J. Kang, G. Kotliar, Optical properties of the infinite-layer $La_{1-x}Sr_xNiO_2$ and hidden Hund's physics. *Phys. Rev. Lett.* **126**, 127401 (2021).

13. J. F. Mitchell, A nickelate renaissance. *Front. Phys.* **9**, 813483 (2021).

14. P. Lacorre, Passage from T-type to T′-type arrangement by reducing $R_4Ni_3O_{10}$ to $R_4Ni_3O_8$ ($R$ = La, Pr, Nd). *J. Solid State Chem.* **97**, 495–500 (1992).

15. G. A. Pan, D. Ferenc Segedin, H. LaBollita, Q. Song, E. M. Nica, B. H. Goodge, A. T. Pierce, S. Doyle, S. Novakov, D. Córdova Carrizales, A. T. N′Diaye, P. Shafer, H. Paik, J. T. Heron, J. A. Mason, A. Yacoby, L. F. Kourkoutis, O. Erten, C. M. Brooks, A. S. Botana, J. A. Mundy, Superconductivity in a quintuple-layer square-planar nickelate. *Nat. Mater.* **21**, 160–164 (2022).

16. D. Li, B. Y. Wang, K. Lee, S. P. Harvey, M. Osada, B. H. Goodge, L. F. Kourkoutis, H. Y. Hwang, Superconducting dome in $Nd_{1-x}Sr_xNiO_2$ infinite layer films. *Phys. Rev. Lett.* **125**, 027001 (2020).

17. S. Zeng, C. S. Tang, X. Yin, C. Li, M. Li, Z. Huang, J. Hu, W. Liu, G. J. Omar, H. Jani, Z. S. Lim, K. Han, D. Wan, P. Yang, S. J. Pennycook, A. T. S. Wee, A. Ariando, Phase diagram and superconducting dome of infinite-layer $Nd_{1-x}Sr_xNiO_2$ thin films. *Phys. Rev. Lett.* **125**, 147003 (2020).

18. M. Gabay, S. Gariglio, J.-M. Triscone, Functionally doped infinite-layer nickelates. *Nat. Mater.* **21**, 139–140 (2022).

19. J. Lee, G. Luo, I.-C. Tung, S. Chang, Z. Luo, M. Malshe, M. Gadre, A. Bhattacharya, S. Nakhmanson, J. Eastman, H. Hong, J. Jellinek, D. Morgan, D. D. Fong, J. W. Freeland, Dynamic

layer rearrangement during growth of layered oxide films by molecular beam epitaxy. *Nat. Mater.* **13**, 879–883 (2014).

20. M. Crespin, P. Levitz, L. Gatineau, Reduced forms of $LaNiO_3$ perovskite. Part 1.—Evidence for new phases: $La_2Ni_2O_5$ and $LaNiO_2$. *J. Chem. Soc. Faraday Trans. 2* **79**, 1181–1194 (1983).

21. K. Lee, B. H. Goodge, D. Li, M. Osada, B. Y. Wang, Y. Cui, L. F. Kourkoutis, H. Y. Hwang, Aspects of the synthesis of thin film superconducting infinite-layer nickelates. *APL Mater.* **8**, 041107 (2020).

22. G. A. Pan, Q. Song, D. F. Segedin, M.-C. Jung, H. El-Sherif, E. E. Fleck, B. H. Goodge, S. Doyle, D. C. Carrizales, P. Shafer, H. Paik, L. F. Kourkoutis, I. E. Baggari, A. S. Botana, C. M. Brooks, J. A. Mundy, Synthesis and electronic properties of $Nd_{n+1}Ni_nO_{3n+1}$ Ruddlesden-Popper nickelate thin films. *Phys. Rev. Mater.* **6**, 055003 (2022).

23. Y. Ji, X. Gao, J. Liu, L. Li, K. Chen, Z. Liao, Stoichiometry, orbital configuration, and metal-to-insulator transition in $Nd_{0.8}Sr_{0.2}NiO_3$ films. *ACS Appl. Mater. Interfaces* **15**, 11353–11359 (2023).

24. Z. Li, W. Guo, T. Zhang, J. Song, T. Gao, Z. Gu, Y. Nie, Epitaxial growth and electronic structure of Ruddlesden–Popper nickelates ($La_{n+1}Ni_nO_{3n+1}$, $n$ = 1–5). *APL Mater.* **8**, 091112 (2020).

25. J. Lee, I. Tung, S.-H. Chang, A. Bhattacharya, D. Fong, J. Freeland, H. Hong, In situ surface/interface x-ray diffractometer for oxide molecular beam epitaxy. *Rev. Sci. Instrum.* **87**, 013901 (2016).

26. H. Sun, Z. Mao, T. Zhang, L. Han, T. Zhang, X. Cai, X. Guo, Y. Li, Y. Zang, W. Guo, J. Song, D. Ji, C. Gu, C. Tang, Z. Gu, N. Wang, Y. Zhu, D. Schlom, Y. Nie, X. Pan, Chemically specific termination control of oxide interfaces via layer-by-layer mean inner potential engineering. *Nat. Commun.* **9**, 2965 (2018).

27. M. Sullivan, M. Ward, A. Gutiérrez-Llorente, E. R. Adler, H. Joress, A. Woll, J. Brock, Complex oxide growth using simultaneous in situ reflection high-energy electron diffraction and x-ray reflectivity: When is one layer complete? *Appl. Phys. Lett.* **106**, 031604 (2015).

28. X. Yan, F. Wrobel, Y. Li, H. Zhou, H.-h. Wang, A. Bhattacharya, J. Sun, H. Hong, D. D. Fong, In situ x-ray and electron scattering studies of oxide molecular beam epitaxial growth. *APL Mater.* **8**, 101107 (2020).

29. Y. Nie, Y. Zhu, C.-H. Lee, L. F. Kourkoutis, J. A. Mundy, J. Junquera, P. Ghosez, D. Baek, S. Sung, X. X. Xi, K. Shen, D. Muller, D. Schlom, Atomically precise interfaces from non-stoichiometric deposition. *Nat. Commun.* **5**, 4530 (2014).

30. W. Wei, K. Shin, H. Hong, Y. Shin, A. S. Thind, Y. Yang, R. F. Klie, F. J. Walker, C. H. Ahn, Solid state reduction of nickelate thin films. *Phys. Rev. Mater.* **7**, 013802 (2023).

31. J. Haeni, C. Theis, D. Schlom, W. Tian, X. Pan, H. Chang, I. Takeuchi, X.-D. Xiang, Epitaxial growth of the first five members of the $Sr_{n+1}Ti_nO_{3n+1}$ Ruddlesden–Popper homologous series. *Appl. Phys. Lett.* **78**, 3292–3294 (2001).

32. Y. Yacoby, M. Sowwan, E. Stern, J. O. Cross, D. Brewe, R. Pindak, J. Pitney, E. M. Dufresne, R. Clarke, Direct determination of epitaxial interface structure in $Gd_2O_3$ passivation of GaAs. *Nat. Mater.* **1**, 99–101 (2002).

33. D. Ferenc Segedin, B. H. Goodge, G. A. Pan, Q. Song, H. LaBollita, M.-C. Jung, H. El-Sherif, S. Doyle, A. Turkiewicz, N. K. Taylor, J. A. Mason, A. T. N′Diaye, H. Paik, I. E. Baggari, A. S. Botana, L. F. Kourkoutis, C. M. Brooks, J. A. Mundy, Limits to the strain engineering of layered square-planar nickelate thin films. *Nat. Commun.* **14**, 1468 (2023).

34. M. Osada, K. Fujiwara, T. Nojima, A. Tsukazaki, Improvement of superconducting properties in $La_{1-x}Sr_xNiO_2$ thin films by tuning topochemical reduction temperature. *Phys. Rev. Mater.* **7**, L051801 (2023).

35. Z. Wang, G.-M. Zhang, Y.-f. Yang, F.-C. Zhang, Distinct pairing symmetries of superconductivity in infinite-layer nickelates. *Phys. Rev. B* **102**, 220501 (2020).

36. N. N. Wang, M. W. Yang, Z. Yang, K. Y. Chen, H. Zhang, Q. H. Zhang, Z. H. Zhu, Y. Uwatoko, L. Gu, X. L. Dong, J. P. Sun, K. Jin, J.-G. Cheng, Pressure-induced monotonic enhancement of $T_c$ to over 30 K in superconducting $Pr_{0.82}Sr_{0.18}NiO_2$ thin films. *Nat. Commun.* **13**, 4367 (2022).

37. G. Krieger, L. Martinelli, S. Zeng, L. Chow, K. Kummer, R. Arpaia, M. M. Sala, N. B. Brookes, A. Ariando, N. Viart, M. Salluzzo, G. Ghiringhelli, D. Preziosi, Charge and spin order dichotomy in $NdNiO_2$ driven by the capping layer. *Phys. Rev. Lett.* **129**, 027002 (2022).

38. F. Lechermann, Emergent flat-band physics in $d^{9-\delta}$ multilayer nickelates. *Phys. Rev. B* **105**, 155109 (2022).

39. S. Kunisada, S. Isono, Y. Kohama, S. Sakai, C. Bareille, S. Sakuragi, R. Noguchi, K. Kurokawa, K. Kuroda, Y. Ishida, S. Adachi, R. Sekine, T. K. Kim, C. Cacho, S. Shin, T. Tohyama, K. Tokiwa, T. Kondo, Observation of small Fermi pockets protected by clean $CuO_2$ sheets of a high-$T_C$ superconductor. *Science* **369**, 833–838 (2020).

40. A. Ikeda, Y. Krockenberger, H. Irie, M. Naito, H. Yamamoto, Direct observation of infinite $NiO_2$ planes in $LaNiO_2$ films. *Appl. Phys. Express* **9**, 061101 (2016).

41. M. Osada, B. Y. Wang, K. Lee, D. Li, H. Y. Hwang, Phase diagram of infinite layer praseodymium nickelate $Pr_{1-x}Sr_xNiO_2$ thin films. *Phys. Rev. Mater.* **4**, 121801 (2020).

42. Y. Yu, L. Ma, P. Cai, R. Zhong, C. Ye, J. Shen, G. D. Gu, X. H. Chen, Y. Zhang, High-temperature superconductivity in monolayer $Bi_2Sr_2CaCu_2O_{8+\delta}$. *Nature* **575**, 156–163 (2019).

43. Q.-Y. Wang, Z. Li, W.-H. Zhang, Z.-C. Zhang, J.-S. Zhang, W. Li, H. Ding, Y.-B. Ou, P. Deng, K. Chang, J. Wen, C.-L. Song, K. He, J.-F. Jia, S.-H. Ji, Y.-Y. Wang, L.-L. Wang, X. Chen, X.-C. Ma, , Q.-K. Xue, Interface-induced high-temperature superconductivity in single unit-cell FeSe films on $SrTiO_3$. *Chinese Phys. Lett.* **29**, 037402 (2012).

44. S. Tan, Y. Zhang, M. Xia, Z. Ye, F. Chen, X. Xie, R. Peng, D. Xu, Q. Fan, H. Xu, J. Jiang, T. Zhang, X. Lai, T. Xiang, J. Hu, B. Xie, D. Feng, Interface-induced superconductivity and strain-dependent spin density waves in $FeSe/SrTiO_3$ thin films. *Nat. Mater.* **12**, 634–640 (2013).

45. J. Lee, F. Schmitt, R. Moore, S. Johnston, Y.-T. Cui, W. Li, M. Yi, Z. Liu, M. Hashimoto, Y. Zhang, D. H. Lu, T. P. Devereaux, D.-H. Lee, Z.-X. Shen, Interfacial mode coupling as the origin of the enhancement of $T_c$ in FeSe films on $SrTiO_3$. *Nature* **515**, 245–248 (2014).

46. B. H. Goodge, B. Geisler, K. Lee, M. Osada, B. Y. Wang, D. Li, H. Y. Hwang, R. Pentcheva, L. F. Kourkoutis, Resolving the polar interface of infinite-layer nickelate thin films. *Nat. Mater.* **22**, 466–473 (2023).

47. B.-X. Wang, H. Zheng, E. Krivyakina, O. Chmaissem, P. P. Lopes, J. W. Lynn, L. C. Gallington, Y. Ren, S. Rosenkranz, J. Mitchell, D. Phelan, Synthesis and characterization of bulk $Nd_{1-x}Sr_xNiO_2$ and $Nd_{1-x}Sr_xNiO_3$. *Phys. Rev. Mater.* **4**, 084409 (2020).

48. P. Puphal, Y.-M. Wu, K. Fürsich, H. Lee, M. Pakdaman, J. A. Bruin, J. Nuss, Y. E. Suyolcu, P. A. van Aken, B. Keimer, M. Isobe, M. Hepting, Topotactic transformation of single crystals: From perovskite to infinite-layer nickelates. *Sci. Adv.* **7**, eabl8091 (2021).

49. H. Sun, M. Huo, X. Hu, J. Li, Z. Liu, Y. Han, L. Tang, Z. Mao, P. Yang, B. Wang, J. Cheng, D.-X. Yao, G.-M. Zhang, M. Wang, Signatures of superconductivity near 80 K in a nickelate under high pressure. *Nature* **621**, 493–498 (2023).

50. H. S. Kum, H. Lee, S. Kim, S. Lindemann, W. Kong, K. Qiao, P. Chen, J. Irwin, J. H. Lee, S. Xie, S. Subramanian, J. Shim, S.-H. Bae, C. Choi, L. Ranno, S. Seo, S. Lee, J. Bauer, H. Li, K. Lee, J. A. Robinson, C. A. Ross, D. G. Schlom, M. S. Rzchowski, C.-B. Eom, J. Kim, Heterogeneous integration of single-crystalline complex-oxide membranes. *Nature* **578**, 75–81 (2020).

51. G.-M. Zhang, Y.-f. Yang, F.-C. Zhang, Self-doped Mott insulator for parent compounds of nickelate superconductors. *Phys. Rev. B* **101**, 020501 (2020).

52. K. Lee, B. Y. Wang, M. Osada, B. H. Goodge, T. C. Wang, Y. Lee, S. Harvey, W. J. Kim, Y. Yu, C. Murthy, S. Raghu, L. F. Kourkoutis, H. Y. Hwang, Linear-in-temperature resistivity for optimally superconducting (Nd,Sr)$NiO_2$. *Nature* **619**, 288–292 (2023).